JPET Fast Forward. Published on August 2, 2017 as DOI: 10.1124/jpet.117.242735
This article has not been copyedited and formatted. The final version may differ from this version.

JPET #242735

CXCR4-specific Nanobodies as potential therapeutics for WHIM syndrome

Raymond H. de Wit, Raimond Heukers, Hendrik Brink, Angela Arsova[1], David Maussang[2], Pasquale Cutolo, Beatrijs Strubbe, Henry F. Vischer, Françoise Bachelerie and Martine J. Smit

Division of Medicinal Chemistry, Amsterdam Institute for Molecules Medicines and Systems (AIMMS), Vrije Universiteit Amsterdam, De Boelelaan 1108, 1081 HZ Amsterdam, The Netherlands (R.H.d.W., R.H., H.B., A.A., D.M., R.L., H.F.V, M.J.S.)

Inflammation Chemokines and Immunopathology, INSERM, Fac. de medicine-Univ Paris-Sud, Universite Paris-Saclay, Clamart, France (P.C., F.B.)

Ablynx NV, Zwijnaarde, Belgrium (B.S.)

JPET Fast Forward. Published on August 2, 2017 as DOI: 10.1124/jpet.117.242735
This article has not been copyedited and formatted. The final version may differ from this version.

A. Running title: CXCR4-Nanobodies as potential therapeutics

B. Correspondence to:

Martine J. Smit

Amsterdam Institute for Molecules, Medicines and Systems

Division of Medicinal Chemistry

Vrije Universiteit Amsterdam

De Boelelaan 1108

1081 HZ Amsterdam, The Netherlands

Tel.: +31205987572

E-mail: mj.smit@vu.nl

C.

Number of pages: 39

Number of tables: 2

Number of figures: 4

Number of references: 59

Number of words in Abstract: 250

Number of words in Introduction: 748

Number of words in Discussion: 1067

D. Abbreviations:

G protein-coupled receptor (GPCR), extracellular loop 2 (ECL2), human papillomavirus (HPV), inositol phosphate (IP), Nanobody (Nb), phospholipase C (PLC), warts, hypogammaglobulinemia, infections and myelokathexis (WHIM)

E. Recommended section assignment: Cellular and Molecular

JPET Fast Forward. Published on August 2, 2017 as DOI: 10.1124/jpet.117.242735
This article has not been copyedited and formatted. The final version may differ from this version.

ABSTRACT

WHIM syndrome is a rare congenital immunodeficiency disease, named after its main clinical manifestations: Warts, Hypogammaglobulinemia, Infections and also Myelokathexis, which refers to abnormal accumulation of mature neutrophils in the bone marrow. The disease is primarily caused by C-terminal truncation mutations of the chemokine receptor CXCR4 giving these CXCR4-WHIM mutants a gain of function in response to their ligand CXCL12. Considering the broad functions of CXCR4 in maintaining leukocytes homeostasis, patients are panleukopenic and display altered immune responses, likely as a consequence of impairment in the differentiation and trafficking of leukocytes. Treatment of WHIM patients currently consists of symptom relief, leading to unsatisfactory clinical responses. As an alternative and potentially more effective approach, we tested the potency and efficacy of CXCR4-specific Nanobodies on inhibiting CXCR4-WHIM mutants. Nanobodies® are therapeutic proteins based on the smallest functional fragments of heavy chain antibodies. They combine the advantages of small-molecule drugs and antibody-based therapeutics due to their relative small size, high stability and high affinity. We compared the potential of monovalent and bivalent CXCR4-specific Nanobodies to inhibit CXCL12-induced CXCR4-WHIM-mediated signaling with the small molecule clinical candidate AMD3100. The CXCR4-targeting Nanobodies displace CXCL12 binding and bind CXCR4-WT and -WHIM (R334X/S338X) mutants and with (sub-) nanomolar affinities. The Nanobodies' epitope was mapped to the extracellular loop 2 of CXCR4, overlapping with the binding site of CXCL12. Monovalent, and in particular bivalent Nanobodies were more potent than AMD3100 in reducing CXCL12-mediated G protein activation. In addition, CXCR4-WHIM-dependent calcium flux and wound healing of HPV-immortalized cell lines in response to CXCL12 was effectively inhibited by the Nanobodies. Based on these *in vitro* results, we conclude that CXCR4 Nanobodies hold significant potential as alternative therapeutics for CXCR4-associated diseases like WHIM syndrome.

JPET Fast Forward. Published on August 2, 2017 as DOI: 10.1124/jpet.117.242735
This article has not been copyedited and formatted. The final version may differ from this version.

INTRODUCTION

WHIM syndrome is a rare congenital immunodeficiency disease caused by aberrant activity of the chemokine CXCL12/CXCR4 axis (Hernandez et al., 2003; Bachelerie, 2010). The disease is named after its main four clinical manifestations: Human Papilloma virus (HPV)-induced Warts, Hypogammaglobulinemia, recurrent bacterial Infections and Myelokathexis (Gorlin et al., 2000; Hernandez et al., 2003). WHIM syndrome patients are generally panleukopenic and display a combination of WHIM syndrome-induced immunodeficiencies (Kawai and Malech, 2009; McDermott et al., 2011a). In addition to a selective susceptibility to HPV-mediated pathogenesis (cutaneous and genital warts that cannot be controlled and might progress to cancer), patients are prone to recurrent bacterial infections and can develop various malignancies, including Epstein-Barr virus-associated lymphoproliferative diseases or primary cutaneous follicle center lymphoma (Imashuku et al., 2002; Chow et al., 2010; Beaussant Cohen et al., 2012; Yoshii et al., 2015; Meuris et al., 2016). WHIM syndrome is primarily caused by heterozygous autosomal dominant CXCR4 mutations within the C-terminus of the receptor. Although the mutations are heterogeneous, they are all located in the region encoding for the carboxyl-terminus of the receptor, resulting into four nonsense and four frameshift truncation mutations (Beaussant Cohen et al., 2012; Al Ustwani et al., 2014; Liu et al., 2016) and one single point substitution (E343K) mutation (Liu et al., 2012). The most common WHIM variants are the R334X and S338X truncation mutants, which lack either 19 or 15 residues from the C-terminus (**Table I**) (McDermott et al., 2011b; Ballester et al., 2016). These WHIM mutations render CXCR4 hyperresponsive to its ligand CXCL12 together with impaired desensitization and internalization of the mutant receptor (Balabanian et al., 2005). Interestingly, besides the germline CXCR4 mutations in the WHIM syndrome, somatic WHIM-like mutations are found in 30% of the patients with Waldenström's macroglobulinemia, which have been correlated to tumor progression and drug resistance (Hunter et al., 2014; Roccaro et al., 2014; Kapoor et al., 2015). Interestingly, distinct genetic mechanisms (e.g. germline vs. somatic) are associated with identical or highly similar mutations in the CXCR4 C-terminal region (Liu et al., 2016). CXCR4 is widely expressed on leukocytes (Forster et al., 1998; Lee et al., 1999) and plays a role in retention and homing of cells to the bone marrow (Ma et al.,

JPET Fast Forward. Published on August 2, 2017 as DOI: 10.1124/jpet.117.242735
This article has not been copyedited and formatted. The final version may differ from this version.

1999), CXCR4 mutations also affect immunological processes and result in decreased levels of circulating leukocytes and immunoglobulins (Bock et al., 2014; Brault et al., 2014). Considering the broad functions of CXCR4 in maintaining leukocyte homeostasis, patients suffering from the WHIM syndrome display altered immune responses likely as a consequence of impairment in the differentiation and trafficking of leukocytes (McDermott et al., 2015; Biajoux et al., 2016; Freitas et al., 2017).

Currently, WHIM syndrome treatment consists of symptom relief, which does not target the aberrant CXCR4 signaling and are moderately effective. Treatments range from granulocyte colony-stimulating factor to induce the release of immune cells from the bone marrow to prophylactic antibiotics against respiratory bacterial infections and intravenously administered immunoglobulins to compensate the hypogammaglobulinemia (Kawai and Malech, 2009). However, phase 1 clinical studies with the low molecular weight CXCR4 antagonist AMD3100 (plerixafor, Mobozil®) have demonstrated the potential of targeting CXCR4 in WHIM syndrome therapy (Dale et al., 2011; McDermott et al., 2011a; McDermott et al., 2014a). AMD3100 is an FDA-approved drug for stem-cell mobilisation in non-Hodgkin's lymphoma and multiple myeloma. In addition, AMD3100 treatment effectively corrected panleukopenia (McDermott et al., 2011a), decreased the disease burden and was relatively safe for relatively long term (6 months) and low dose use in WHIM patients (McDermott et al., 2014a). However, in a different setting, single-dose or short term AMD3100 treatment was also associated with side effects such as: abdominal bloating, diarrhea, headache, nausea, lightheadedness, facial paresthesias and injection-site erythema (Liles et al., 2003; Devine et al., 2004). Long term AMD3100 treatment for HIV-infections were discontinued due to potential cardiac toxicity (Scozzafava et al., 2002; De Clercq, 2003). AMD3100 is also associated with suboptimal pharmacokinetic characteristics, such as a short *in vivo* half-life (3.5h) and limited oral bioavailability (Hendrix et al., 2000). Altogether, this illustrates that treating WHIM syndrome by targeting CXCR4 might be effective but with the need to target it more safely.

The nanobody platform provides an alternative strategy to target CXCR4-WHIM signaling. Nanobodies are 12-15 kDa recombinant single-domain antibody fragments and have advantages over small

JPET Fast Forward. Published on August 2, 2017 as DOI: 10.1124/jpet.117.242735
This article has not been copyedited and formatted. The final version may differ from this version.

molecule drugs in terms of target affinity and specificity. Another benefit of Nanobodies is their modular structure, which conveniently allows the generation of multivalent nanobody formats to improve functional affinity, increase *in vivo* half-life, bispecific targeting and/or allow tissue specific-targeting (Els Conrath et al., 2001; Mujic-Delic et al., 2014). Because of their size and molecular structure, Nanobodies more readily recognize buried epitopes (e.g. GPCR ligand-binding pockets) as compared to conventional antibodies, have high protein stability and low immunogenicity (Steyaert and Kobilka, 2011; Mujic-Delic et al., 2014; Peyvandi et al., 2016). Previously, we described CXCR4-specific Nanobodies that antagonized CXCL12-dependent binding/signaling and inhibited HIV-infection (Jahnichen et al., 2010). In this study, we evaluated the potential of CXCR4-targeting Nanobodies as WHIM syndrome therapeutics and compared their potencies in their ability to displace CXCL12 binding and inhibit CXCL12-induced signaling of both CXCR4-WT and -WHIM mutants.

JPET Fast Forward. Published on August 2, 2017 as DOI: 10.1124/jpet.117.242735
This article has not been copyedited and formatted. The final version may differ from this version.

MATERIALS AND METHODS

Materials

The CXCR4 ligands, recombinant human CXCL12 was obtained from Peprotech (Rocky Hill, NJ, USA) and AMD3100 (1,1'-[1,4-phenylenebis-(methylene)]-bis-1,4,8,11-tetraazacyclotetra-decane) from Sigma-Aldrich (St. Louis, MO, USA). 12G5 monoclonal CXCR4 antibody was purchased from R&D systems (Minneapolis, MN, USA). Linear 25 kDa polyethylenimine for transient transfections was from Polysciences (Eppelheim, Germany). Dulbecco's modified Eagle's medium (DMEM) and Trypsin-EDTA were purchased from Sigma-Aldrich. Fetal bovine serum (FBS), penicillin/streptomycin were obtained from PAA Laboratories GmbH (Paschen, Austria). For coating of cell culture plates, poly-L-lysine solution was obtained from Sigma-Aldrich. ^{125}I-CXCL12 (2200 Ci/mmol) and myo-[2-^{3}H]inositol (1 mCi/ml) were obtained from Perkin Elmer Life Sciences (Boston, MA, USA). Phospho-ERK1/2 (Thr202/Tyr204, #9106 and #4370), total ERK1/2 (#9102) and anti-Myc tag (9B11, #2276) antibodies were from Cell Signaling Technology (Danvers, MA, USA). Anti-rabbit and anti-mouse horseradish peroxidase (HRP)-conjugated antibodies were obtained from Bio-Rad Laboratories (Hercules, CA, USA). Anti-mouse Alexa Fluor® 488-conjugated antibody (A11001) was from Thermo Fisher Scientific (Waltham, MA, USA).

Phage-display selection

Immunization, construction of the nanobody phages libraries and phage-display selections were performed as described previously (Jahnichen et al., 2010).

Molecular biology and nanobody production

pcDNA3.1-CXCR4-WT (GenBank: AF025375.1), a gift from dr. C. P. Tensen (Leiden University Medical Center, Leiden, the Netherlands), was used as template DNA to generate CXCR4-WT, CXCR4-R334X and CXCR4-S338X by PCR using specific primers. The primer sequences were: WT-FW: 5'-CAG GTACCGCCACCATGGAGGGGATCAGTATATACACT-3', WT-REV: 5'-ATTTCTAATTAGCTGGAGTGAAAACTTGAAGA-3',

R334X-REV: 5'- CCCCTCTAGATCACTTTCCTTTGGAGAGGATCTTGAGG-3' and

S338X-REV: 5'-TTTTCTAGATTAATGTCCACCTCGCTTTCCTTTG-3'.

The forward primer encodes a 5' KpnI restriction site, whereas the reverse primers encode 3' XbaI restriction site. The amplified PCR fragments and the mammalian expression vector $pcDEF_3$ (gift from J. A. Langer from Robert Wood Johnson Medical School, Piscataway, NJ) were digested with KpnI and XbaI enzymes and the fragments were ligated into $pcDEF_3$ using T4 DNA ligase. The point-mutated CXCR4 constructs D187V, F189V and V196E in pcDNA3 were kindly provided by Ablynx N.V. The mutants were subcloned to the $pcDEF_3$ vector by PCR, the template DNA was amplified and restriction sites were added by using the F-WT and R-WT primers. All generated DNA constructs were verified by sequencing. All enzymes and buffers used for cloning were obtained from Thermo Fisher Scientific. For nanobody production, BL21 *E. coli* cells were transformed with 10A10-PAX100 and 10A10-35GS-10A10-PAX100 DNA. Periplasmic nanobody expression was induced by addition of 1 mM isopropyl-β-D-thiogalactopyranoside (IPTG, Sigma-Aldrich) to the culture medium. Periplasmic extracts were obtained by a freeze-thaw cycle of the cell pellet and resuspension in phosphate-buffered saline (PBS). The His_6-tagged Nanobodies were purified from the periplasmic extract by ion-metal affinity chromatography using Ni-NTA agarose resin (Thermo Fisher Scientific) according to manufacturer's instructions. Finally, a buffer exchange to PBS was performed by SnakeSkin (Thermo Fisher Scientific) dialysis or PD-10 desalting columns (GE healthcare, Little Chalfront, UK).

Cell Culture

The human embryonic kidney cell line HEK293T was cultured in DMEM (Sigma-Aldrich, St. Louis, MO, USA). The human leukemic K562 cell lines: parental, pcDNA3.1-CXCR4-WT and pcDNA3.1-CXCR4-R334X were previously described(McDermott et al., 2011b) and a kind gift from David McDermott and Philip Murphy (NIH, Bethesda, MD, USA), the cells were cultured in RPMI-1640 (Sigma-Aldrich, St. Louis, MO, USA) The stably transfected K562 cells were cultured with 0.4 mg/ml G418 (Duchefa, Haarlem, the Netherlands) for selection. All growth media was supplemented with 10% (v/v) fetal bovine

JPET Fast Forward. Published on August 2, 2017 as DOI: 10.1124/jpet.117.242735
This article has not been copyedited and formatted. The final version may differ from this version.

serum (FBS), 50 IU/ml penicillin and 50 µg/ml streptomycin (PAA Laboratories GmbH, Paschen, Austria). Cells were grown at 37°C in a humidified atmosphere with 5% CO_2 and passaged two times per week. Transient transfections were performed using the polyethylenimine (PEI) method (Schlaeger and Christensen, 1999).

^{125}I-CXCL12 displacement

Two million HEK293T cells were seeded in 10 cm cell culture dishes. After O/N cell growth the cells were transiently transfected with 250 ng hCXCR4-WT, hCXCR4-R334X or hCXCR4-S338X pcDEF3 supplemented to 5 µg using empty pcDEF3 vector. 48 hours post-transfection the CXCR4-expressing cell membranes were isolated as previously described (de Wit et al., 2016). Radioligand displacement assays were performed as previously described (de Wit et al., 2016). Briefly, in 96-well plates, approximately 75 pM ^{125}I-CXCL12 in HEPES Binding Buffer (50mM HEPES–HCl, pH 7.4, 1 mM $CaCl_2$, 5 mM $MgCl_2$, 0.1 M NaCl, 0.5% (w/v) BSA) was added to increasing concentrations of unlabeled CXCL12, AMD3100, 10A10 or 10A10-10A10 Nanobodies. Radioligand only and radioligand + 100 nM CXCL12 were used as total binding and non-specific binding controls to each assay plate. The ligands were incubated with 5 µg/well CXCR4 (WT, R334X, S338X) or Mock HEK293T membranes for 2 hours at 20˚C to reach binding equilibrium. The radioligand-bound membranes were harvested on 0.5% (w/v) PEI soaked GF/C filter plates (Perkin-Elmer) and dried for 30 minutes at 60°C. Scintillation fluid (MicroScint™-O, Perkin-Elmer) was added and radioactivity was measured using a MicroBeta liquid scintillation counter (Perkin-Elmer). In addition to the radioligand competition plates, the fixed amount of radioligand is also directly added to a GF/C filter plate during each experiment, in order to determine the radioligand concentration in the displacement assay. The data was plotted and analyzed using a Competitive One-Site homologous binding fit for homologous displacement and Competitive One-Site FitLogIC50 binding fit for heterologous displacement with GraphPad Prism 6 software (GraphPad software Inc, San Diego, CA, USA).

JPET Fast Forward. Published on August 2, 2017 as DOI: 10.1124/jpet.117.242735
This article has not been copyedited and formatted. The final version may differ from this version.

Cell surface expression ELISA

Transiently transfected HEK293T cells (6.10^4 were seeded in poly-L-lysine coated 96-well cell culture plates and grown at 37°C. 48 hours post-transfection, cells were fixed for 5 min with 4% formaldehyde (Sigma-Aldrich) in PBS. The cells were washed with PBS and incubated with blocking buffer (5% fat-free milk powder (Sigma-Aldrich) diluted in PBS) for 1h. This was followed by incubation with mouse-anti-CXCR4 (clone 12G5), diluted 1:200 in blocking buffer during 1 hours. After each antibody incubation the cells were washed three times with PBS. Next, the cells were incubated for 1h with the Goat Anti-Mouse IgG (H + L)-HRP Conjugate antibody (Bio-Rad, 1:2500). For colorimetric detection, OPD substrate solution (2 mM o-phenylenediamine (Sigma-Aldrich) in 35 mM citric acid, 66 mM Na_2HPO_4, 0.015% H_2O_2, pH 5.6) was added to the cells. The reaction was terminated after 5 minutes by adding H_2SO_4 (1 M) and absorbance (490 nm) was measured in a PowerWave plate reader (BioTek).

Immunofluorescence microscopy imaging

Transiently transfected (Mock or CXCR4) HEK293T cells (6.10^4 were seeded in poly-L-lysine coated 96-well cell culture plates and grown at 37°C. 48 hours post-transfection, cells were fixed for 5 min with 4% formaldehyde (Sigma-Aldrich) in PBS. The cells were washed with PBS and, if necessary, permeabilized with 0.5% (v/v) NP-40 substituted in PBS for 30 minutes at 20°C. Cells were incubated with blocking buffer (5% (w/v) BSA in in PBS) for 1h. This was followed by 10A10-10A10 (100 nM in blocking buffer) incubation for 1 hour at 20°C. After each nanobody/antibody incubation the cells were washed three times with PBS. Subsequently, Myc-tag antibody (1:1000 in blocking buffer) and the secondary anti-mouse Alexa Fluor® 488-conjugated antibody (1:500 in blocking buffer) was applied for 1 hour at 20°C. Cell nuclei were stained using 4',6-diamidino-2-phenylindole (DAPI) (1 μg/ml) in PBS for 5 minutes at 20°C. Immunofluorescence imaging was carried out using a Olympus FSX-100 microscope.

Cell surface radioligand binding

JPET Fast Forward. Published on August 2, 2017 as DOI: 10.1124/jpet.117.242735
This article has not been copyedited and formatted. The final version may differ from this version.

Transiently transfected (Mock, hCXCR4-WT, mCXCR4-WT, hCXCR7) HEK293T cells were seeded in poly-L-lysine coated 96-well cell culture plates. 48 hours after transfection the culture medium was removed and de cells were incubated with 75 pM ^{125}I-CXCL12 with/without cold ligands (CXCL12, AMD3100, 10A10) in HBB with 0.5% (w/v) BSA and incubated at 4°C for 3 hours until binding equilibrium is reached. The cells were washed three times with ice-cold HEPES wash buffer (HBB + 0.5 M NaCl). Cells were lysed with RIPA buffer, the cell lysate was transferred to radioactivity counting vials and measured with a Compugamma counter (Wallac).

SDS-PAGE and Western blotting

Transiently transfected (Mock, CXCR4-WT, CXCR4-R334X or CXCR4-S338X) HEK293T cells (3.10^5) cells were grown on a 12-well plate on full medium. Cells were synchronized by serum starvation with 0% FBS DMEM and grown overnight. Synchronized cells were treated with CXCL12 (1 nM), AMD3100 (10 μM), 10A10 (1 μM) and/or 10A10-10A10 (100 nM). For CXCL12 inhibition experiments, the cells were pre-incubated for 1h at 37°C with the CXCR4-inhibitors prior to CXCL12 stimulation (1 nM). After 5 or 15 minutes of CXCL12 stimulation the cells were lysed on ice with RIPA buffer supplemented with 1 mM NaF, 1 mM $NaVO_4$ and protease inhibitor cocktail (cOmplete, Roche), sonicated and centrifuged to remove insoluble cell debris. Protein content of the lysates was determined using a BCA protein estimation assay according to manufacturer's instructions (Thermo Fisher Scientific). Equal amounts of protein were resolved by SDS-PAGE analysis using 10% acrylamide gels. After electrophoresis, protein was to PVDF membranes (Bio-Rad), which was subsequently blocked for 1h at 22°C in 5% non-fat milk in 0.1% Tween-20/TBS solution. Western blot was performed according to standard procedure and blotted against Phospho-ERK1/2 (Thr202/Tyr204, #9106 and #4370, 1:1000), total ERK1/2 (#9102, 1:1000) (Cell Signaling Technology) or β-actin (Sigma-Aldrich, #A5316, 1:2500). Next the membranes were incubated with secondary anti-Mouse or anti-Rabbit HRP-conjugated antibodies (Bio-Rad, 1:5000) The Western blot

images were acquired by chemiluminescence (ECL solution, Perkin-Elmer) and a Chemi Doc imager (Bio-Rad), the signal was quantified by densitometry using Image lab Software (Bio-Rad).

Flow cytometry

HEK293T cells were transiently transfected in with 100 ng hCXCR4-WT, D187V, F189V or V196E receptor DNA, supplemented to 5 µg with empty pcDEF$_3$ DNA. 24 h post transfection cells were dissociated with non-enzymatic cell dissociation buffer (Sigma-Aldrich). 1.10^5 cells/well were seeded at in clear 96-well U-bottom plates in assay buffer (ice-cold phosphate buffered saline (PBS) supplemented with 5% FBS). After which cells were incubated with increasing concentrations of 10A10-10A10 Nanobodies in assay buffer at 4°C. Cells were washed three times with ice-cold assay buffer. Subsequently, cells were incubated with the primary Myc-tag antibody (Cell Signaling Technology, 9B11, #2276, 1:1000) in assay buffer for 1h at 4°C. Cells were washed three times with ice-cold assay buffer. Finally, cells were incubated with the secondary fluorescent anti-mouse IgG (H+L) polyclonal antibody Alexa 488 (Thermo Fisher Scientific, A11001) for 1 h at 4°C. Afterwards, cells were washed three times with ice-cold assay buffer. Fluorescence-assisted flow cytometry was performed on a Guava Easycyte (Guava Technologies, MERCK Millipore). Data was analyzed using GraphPad Prism version 6.0 (GraphPad Software, Inc., La Jolla, CA, USA). Specific binding plotted as mean fluorescent counts of ungated samples. Background subtraction of unspecific binding was performed using values obtained from the mock-transfected samples. Curves were fitted using one site-specific binding algorithm (Y = Bmax*X/(Kd + X)) in GraphPad Prism 6.0.

Phospholipase C activation

HEK293T cells (4.10^6) were transiently transfected with 100 ng hCXCR4-WT, R334X or S338X receptor DNA, 2.5 µg $G\alpha_{qi5}$ DNA and 2.4 µg pcDEF$_3$ DNA. 24h post-transfection, cells ($1.2.10^5$/well) seeded at in poly-L-lysine coated flat bottom 48-wells plates and labeled overnight with myo-[2-3H]-inositol (1 µCi/mL) in Earle's inositol-free minimal essential medium supplemented with 10% FBS and 1% P/S. The next day, the labeling medium was aspirated and the cells were stimulated with CXCL12 (agonist mode)

JPET Fast Forward. Published on August 2, 2017 as DOI: 10.1124/jpet.117.242735
This article has not been copyedited and formatted. The final version may differ from this version.

in assay buffer (20 mM HEPES, 140 mM NaCl, 5 mM KCl, 1 mM $MgSO_4$, 1 mM $CaCl_2$, 10 mM glucose) supplemented with 0.05% BSA and 10 mM LiCl. In case of antagonist-mode experiments, the cells were pre-incubated with antagonist solutions in assay buffer supplemented with 0.05% BSA for 5 minutes at 20°C, prior to addition of 5 nM (EC_{80}) CXCL12 solutions in assay buffer supplemented with 0.05% BSA and 10 mM LiCl. After 1.5h incubation at 37°C the inositol-phosphates accumulation was terminated by placing the cells on ice and aspirating the stimulation buffer prior to the addition of ice-cold 10 mM formic acid to permeabilize the cells. After 1h incubation on ice, the [^{3}H]-inositol phosphates (InsP) were isolated by anion-exchange chromatography (Dowex AG1-X8 columns; Bio-Rad) to counting vials. Scintillation fluid (Perkin-Elmer) was added and the samples were counted by a Packard TriCarb liquid scintillation analyzer (2 min/vial). Data was analyzed using GraphPad Prism version 6.0 (*GraphPad Software, Inc., La Jolla, CA, USA*). Agonist mode curves were fitted using dose-response log(agonist) versus response equation (Y=Bottom + (Top Bottom)/(1+10^((LogEC50-X))) in GraphPad Prism version 6.0 (*GraphPad Software, Inc., La Jolla, CA, USA*). CXCL12 EC_{80} values were determined from the obtained EC_{50} values by using the following equation: EC_f = (f/100-f)^1/H * EC_{50}, where f stands for 80 and H is the Hill slope. Antagonist mode, dose-response curves of 10A10 Nanobodies and AMD3100 in competition with a fixed 5 nM CXCL12 were fitted with log(inhibitor) versus response algorithm Y=Bottom + (Top-Bottom)/(1+10^((X-LogIC50))) in GraphPad Prism version 6.0 (*GraphPad Software, Inc., La Jolla, CA, USA*).

Reporter gene

HEK293T cells were transiently transfected with CRE luciferase reporter gene and CXCR4-WT, CXCR4-R334X or CXCR4-S338X. Briefly, 1.10^6 cells were transfected with CXCR4-pcDEF$_3$ (250 ng), 1 µg CRE-luc vector supplemented with empty pcDEF$_3$ vector to a total of 2 µg. Transfected cells were seeded in white bottom 96-well assay plates and grown overnight at 37°C. For agonist mode, the cells are incubated with increasing concentrations (10^{-13}-10^{-7} M) of CXCL12 and 1 µM forskolin in DMEM. For CXCL12 inhibition (antagonist mode), the cells were incubated with 1 nM (EC_{80}), 1 µM forskolin and increasing

JPET Fast Forward. Published on August 2, 2017 as DOI: 10.1124/jpet.117.242735
This article has not been copyedited and formatted. The final version may differ from this version.

concentrations of antagonist (AMD3100, 10A10, 10A10-10A10). After 6 hours stimulation at 37°C, the medium was aspirated and the cells were lysed by addition of 25 µL LAR reagent (0.83 mM ATP, 0.83 mM d-luciferine, 18.7 mM $MgCl_2$, 0.78 µM Na_2HPO_4, 38.9 mM Tris–HCl (pH 7.8), 0.39% glycerol, 0.03% Triton X-100 and 2.6 µM DTT]. Luminescence (1 s per well) was measured in Mithras LB940 multilabel plate reader (Berthold Technologies) after 30 min of incubation at 37°C. The data was plotted and fitted (dose-response stimulation (agonist mode) or dose-response inhibition (antagonist mode), three parameters) using Graphpad Prism version 6.0 (GraphPad Software, Inc., La Jolla, CA, USA).

Intracellular calcium flux

K562 cells were seeded (1.10^5 cells/well, 50 µL) in assay buffer (Hank's balanced saline solution (HBSS, Sigma-Aldrich) supplemented with 0.05% BSA and 20 mM of HEPES at a pH of 7,4) in black clear bottom 96 well plates and allowed to settle for 1 h in a humidified growth chamber at 37°C with 5% CO_2. Afterwards, 20 µL of a 7x concentrated antagonist dilution made in assay buffer was added to the required wells. In the case of agonist-mode, 20 µL of assay buffer was added to the wells. According to manufacturer's instructions (Fluo-4 NW Calcium Assay Kit, Molecular Probes, Thermo Fisher Scientific), intracellular calcium was labeled by the addition of 50 µL of a Fluor-4 NW dye solution prepared in assay buffer and supplemented with 5 mM probenecid acid to each well followed by a 30 minute incubation in the dark at 37°C. Intracellular calcium fluxes were measured on the NOVOstar microplate reader (BMG, Labtech) during a total measurement time span of 110 seconds per well at a temperature of 37°C. Initially, baseline fluorescence was measured for 9 seconds after which cells were stimulated with 20 µL of 7x final concentration CXCL12 solution. The agonist injection time span was 7 seconds and fluorescence measurements thus continued from t=16 seconds. The calcium trace was recorded for 74 seconds (t=90s) after agonist stimulation, after which 50 µL of a 5% (v/v) Triton-X100 (Sigma-Aldrich)/assay buffer was added to lyse cells. The total calcium fluorescence was measured for a duration of 20 seconds until t=110s. Data was subsequently analyzed using GraphPad Prism version 6.0 (GraphPad Software, Inc., La Jolla, CA, USA).

JPET Fast Forward. Published on August 2, 2017 as DOI: 10.1124/jpet.117.242735
This article has not been copyedited and formatted. The final version may differ from this version.

Wound healing assay

Wound-healing assays were performed as described previously (Chow et al., 2010). In short, 1×10^5 HPV18 immortalized human keratinocytes were seeded on gelatin-fibronectin-coated coverslips and were grown to confluence in complete KSFM medium. Cells were scratched and incubated with or without Nanobodies or AMD3100 for 16 hours. Cells were fixed and subsequently stained for polymeric F actin and nuclei using TRITC-tagged phalloidin and Hoechst 33342, respectively. Scratch closure was then visualized by immunofluorescence microscopy. Size of the wound was automatically calculated using the Axiovision 4.6 software.

Data analyses

All data was obtained from at least three independent experiments in triplicates. All bar graphs and statistical analyses were obtained with GraphPad Prism 6 software (GraphPad software Inc, San Diego) Bars and errors represent the mean ± SEM. * indicate p values <0.05 as determined by unpaired t-test.

JPET Fast Forward. Published on August 2, 2017 as DOI: 10.1124/jpet.117.242735
This article has not been copyedited and formatted. The final version may differ from this version.

RESULTS

WHIM syndrome-associated CXCR4 mutations, such as CXCR4-R334X and CXCR4-S338X, possess a truncated C-terminal tail (**Table I**). Homologous CXCL12 radioligand displacement studies on HEK293T membranes showed similar CXCL12 binding affinities for CXCR4-WT, -R334X and -S338X (pK_i values of 10.4 ± 0.4, 10.4 ± 0.8 and 10.0 ± 0.4 respectively, **Fig. 1A**). Next, the effect of WHIM mutations on ligand-induced G protein signaling was assessed. Co-expression of the chimeric G-protein $G\alpha_{qi5}$ redirects CXCR4 signaling from the $G\alpha_i$ pathway to $G\alpha_q$-mediated phospholipase C (PLC) activation, which can be readily quantified via inositol-phosphate (IP) accumulation (Conklin et al., 1993). CXCL12 induced equipotent increases of CXCR4-WT, -R334X or -S338X-mediated IP-accumulation (pEC_{50} values of 8.8 ± 0.1, 8.90 ± 0.07, 8.90 ± 0.08 respectively, **Fig. 1B**), while no effect was observed on mock-transfected cells (**Supplemental Figure 1A**). Moreover, at a similar expression level (**Fig. 1C**) a 2-fold increase in maximum response of CXCL12-induced IP accumulation was observed for the two CXCR4-WHIM receptors, as compared to CXCR4-WT. CXCL12 also results in CXCR4-mediated activation of the MAPK pathway. We therefore compared the CXCL12-induced ERK1/2 activation (phosphorylated at Thr202/Tyr204) by CXCR4-WT and WHIM mutant S338X (**Fig. 1D**). Compared to the WT, CXCR4-S338X displayed a sustained increase in phosphorylation of Thr202/Tyr204 ERK1/2 levels upon CXL12 exposure. Taken together, although CXCL12 binding affinities and potencies are identical between WT and WHIM receptors, the degree of signaling of WHIM receptors is increased and prolonged.

As a novel approach to inhibit the hyperactivation of CXCR4-WHIM mutants, new CXCR4-targeting Nanobodies were selected of which nanobody 10A10 was selected as lead molecule. The Nanobodies were produced as monovalent nanobody and as bivalent nanobody-constructs in which two identical 10A10 Nanobodies were separated by a flexible glycine-serine $(GGGGS)_4$ linker. These Nanobodies allowed a sensitive detection of cell surface and intracellularly localized CXCR4 in immunofluorescence microscopy, without any detectable background staining on mock or non-transfected cells (**Fig. 2A**). Both monovalent and bivalent Nanobodies and the reference compound AMD3100

JPET Fast Forward. Published on August 2, 2017 as DOI: 10.1124/jpet.117.242735
This article has not been copyedited and formatted. The final version may differ from this version.

displaced the radioligand (75 pM of ^{125}I-CXCL12) from CXCR4 in a dose-dependent manner (**Fig. 2B**). The Nanobodies displayed a high potency in displacing CXCL12 from CXCR4-WT (pIC_{50} values of 7.7 ± 0.2 for monovalent and 8.8 ±0.1 for bivalent), compared to AMD3100 (6.3 ± 0.1). The bivalent nanobody construct displayed a 10-fold increase in binding affinity, as compared to its monovalent variant, resulting in nanomolar binding affinity for CXCR4-WT. On the WHIM mutants, both monovalent and bivalent could displace CXCL12 binding (partial for the monovalent and full displacement for the bivalent nanobody**.** The affinities of the monovalent and bivalent Nanobodies for CXCR-WT and -R334X (Fig. 2A, right) or -S338X (**Supplemental Figure 1B**) were comparable (**Table II).**

Human CXCR4 shares high sequence identity (90%) with its murine orthologue and binds the same endogenous chemokine (CXCL12) as the human receptor ACKR3 (31% sequence identity, also referred to as CXCR7) (Gravel et al., 2010). Target-specificity was verified by ^{125}I-CXCL12 displacement assays on intact HEK293T cells transiently transfected with human CXCR4 (hCXCR4), human ACKR3 (hACKR3) or mouse CXCR4 (mCXCR4) (**Fig. 2C**). While 10A10 fully displaced ^{125}I-CXCL12 from hCXCR4, it could not displace CXCL12 from ACKR3 or mCXCR4. This indicates that the nanobody 10A10 is specific for human CXCR4. Variations between human and murine CXCR4 orthologues are predominantly found in their extracellular loop 2 (ECL2) region (**Fig. 2D**). For this reason, we subsequently assessed the binding of 10A10 to ECL2 point-mutants of hCXCR4 (D187V, F189V and V196E) (**Fig. 2E**). These point mutations were previously shown to have no effect on cell surface expression and 12G5 antibody binding (Wang et al., 1998; Jahnichen et al., 2010). While 10A10 showed high affinity binding to both CXCR4-WT (pK_D value of 8.9 ± 0.06) and CXCR4-F189V (pK_D value of 8.7 ± 0.03), a complete lack of binding was observed for the CXCR4-D187V mutant. This indicates an essential role for the acidic residue D187 in binding of 10A10 to CXCR4.

Following the evaluation of 10A10 binding characteristics, the CXCR4 Nanobodies were functionally characterized in CXCR4 signaling assays. The Nanobodies and AMD3100 fully antagonized CXCL12-induced signaling of CXCR4-WT and CXCR4-R334X (**Fig. 3A**) and CXCR4-S338X (**Supplemental Figure 1C**) mutants. However, the Nanobodies showed potencies that were up to 100 fold

JPET Fast Forward. Published on August 2, 2017 as DOI: 10.1124/jpet.117.242735
This article has not been copyedited and formatted. The final version may differ from this version.

greater than that of AMD3100 (**Table II**). We then evaluated the potential of the CXCR4 antagonists to inhibit CXCL12-induced, CXCR4-dependent ERK1/2 activation. Pre-incubation of CXCR4-WT or CXCR4-WHIM (R334X) expressing cells with saturating concentrations (>50x K_D) of CXCR4 antagonist for a period of 1 hour, strongly inhibited the CXCL12-induced ERK1/2 activation after 5 or 15 minute treatments (**Fig. 3B**). CXCR4-mediated signaling via $G\alpha_i$ results in reduced levels of cyclic-AMP (cAMP) associated with reduced CRE (cAMP response element) gene regulation. No differences in potency or efficacy in CXCL12-induced $G\alpha_i$ activation could be detected between WT and the WHIM mutants (**Supplemental Figure 1D**). Inhibition of CXCL12-induced $G\alpha_i$ activation by either the Nanobodies or AMD3100 resulted in a dose-dependent increase in cAMP levels in case of either CXCR4-WT and CXCR4-R334X (**Fig. 3C-D**) and CXCR4-S338X (**Supplemental Figure 1E**). In case of CXCR4-WT, AMD3100 partially inhibited CXCL12-induced CRE-Luc activation, while the bivalent nanobody completely inhibited CXCL12-induced $G\alpha_i$ activation with increased potency (**Table II**). None of the antagonists showed differences in potencies or efficacies between CXCR4-WT and the WHIM mutants.

After these initial pharmacological analyses in HEK293T cells, the CXCR4 Nanobodies were evaluated in more clinically relevant cell lines and assays. Previously, McDermott *et al.* generated CXCR4-WT and CXCR4-R334X overexpressing K652 cell lines, which are of myeloid leukemic origin (McDermott et al., 2011b). Here, we used these cells to study real-time calcium flux responses upon CXCL12 stimulation. First, we analyzed the CXCL12 response in parental K562 cells or K562 cells expressing CXCR4-WT or CXCR4-R334X. The CXCR4-expressing cells clearly displayed an increase in intracellular calcium release upon CXCL12 stimulation, which was not detected in the parental K562 cells (**Fig. 4A**). Moreover, this CXCL12-induced calcium response could be fully inhibited with either AMD3100 (10 μM) or 10A10-10A10 (100 nM) in case of CXCR4-WT and almost fully in case of the CXCR4-R334X mutant) (**Fig. 4B** and **Table II**).

WHIM syndrome has been linked to HPV-associated malignancies (Chow et al., 2010; Beaussant Cohen et al., 2012). Furthermore, HPV18-immortalized human keratinocytes (HK-HPV18) display autocrine CXCL12/CXCR4 signaling that enhances cell migration (Chow et al., 2010). We therefore

JPET Fast Forward. Published on August 2, 2017 as DOI: 10.1124/jpet.117.242735
This article has not been copyedited and formatted. The final version may differ from this version.

assessed the effect of our CXCR4 Nanobodies on migration of these HK-HPV18 cells in a wound healing assay (**Fig. 4C-D**). Without treatment, this wound is closed entirely after 16 hours of culture. The bivalent Nanobodies significantly inhibited this would healing up to 60% in a dose-dependent manner (**Fig. 4D**). In contrast, AMD3100 (25 μM) was only able to reach 26% of wound healing.

To summarize, these data indicate that the CXCR4 Nanobodies effectively antagonize CXCL12 function, with overall superior pharmacological characteristics as compared to AMD3100.

DISCUSSION

In this study, we pharmacologically characterized CXCR4-targeting Nanobodies on CXCR4-WT and WHIM-related CXCR4 mutants. Different WHIM mutants, predominantly varying in the length of their C-terminal tail, have been described that display similar biological phenotypes (Lagane et al., 2008; McCormick et al., 2009; McDermott et al., 2011b; Kallikourdis et al., 2013). The most common WHIM mutants CXCR4-R334X and -S338X were taken along in our study (Beaussant Cohen et al., 2012). Homologous radioligand displacement showed similar binding affinities of CXCL12 for these WHIM mutants as to CXCR4 WT. Yet, WHIM mutants showed a two-fold increase in CXCL12-induced $G\alpha_i$ response and phosphorylation of ERK1/2 activation was sustained. Furthermore, we observed no differences in cell surface expression, ligand binding and signaling between CXCR4-R334X and -S338X receptors. These findings are in line with earlier reports that described increased and sustained signaling of CXCR4-WHIM mutants (Balabanian et al., 2005; Mueller et al., 2013; Cao et al., 2015). CXCR4 is known to be ubiquitously expressed in several cell types, including HEK293T cells, which may complicate studying characteristics of CXCR4 mutants. In our signaling assays using HEK293T cells, we did not observe significant CXCL12 responses (**Supplementary Figure 1A**) in mock-transfected cells, indicating that the data generated with HEK293T-CXCR4 overexpression models was not compromised by endogenous CXCR4 expression.

In small scale WHIM syndrome clinical trials, the FDA approved small molecule CXCR4 antagonist AMD3100/plerixafor appeared relatively safe and effective for WHIM syndrome treatment. We characterized the ability of novel CXCR4-targeting Nanobodies, monovalent and bivalent 10A10, to inhibit the WHIM syndrome phenotype. In this study, AMD3100 was used as a benchmark antagonist of CXCL12-induced CXCR4 signaling. Radioligand displacement assays showed that the bivalent CXCR4-specific Nanobodies 10A10 fully inhibit binding of ^{125}I-CXCL12 to human CXCR4. No differences in displacement was observed between CXCR4-WT and WHIM mutants. With potency values that were 10-fold (monovalent nanobody) and 100-fold (bivalent nanobody) greater than that of AMD3100, the CXCR4-

JPET Fast Forward. Published on August 2, 2017 as DOI: 10.1124/jpet.117.242735
This article has not been copyedited and formatted. The final version may differ from this version.

targeting Nanobodies are superior to AMD3100. The gain in potency observed for the bivalent nanobody is likely due to an increased binding avidity that is obtained by combining two binding affinities in one molecule (Rudnick and Adams, 2009; Vauquelin and Charlton, 2013).

CXCR4 binds to its natural ligand CXCL12 via interactions with the N-terminus and ECL2 of the receptor (Brelot et al., 2000; Cutolo et al., 2017). Within this ECL2, the aspartic acid at position 187 (D187) was previously described to be involved in binding of CXCL12 (Brelot et al., 2000; Jahnichen et al., 2010; Wescott et al., 2016). The D187 residue was also shown to be crucial for binding of the 10A10 CXCR4 nanobody to the receptor. In addition, mutation of the valine at position 196 (V196) caused a 10-fold decrease in affinity. The two previously described, chemokine-competing, CXCR4 Nanobodies 238D4 and 238D2 required either D187 (nanobody 238D4) or V196 (nanobody 238D2) (Jahnichen et al., 2010). The overlap in ECL2 residues involved in binding of either CXCL12, the previously described Nanobodies and our new 10A10 nanobody correlates well with the ability of these Nanobodies to displace CXCL12 from CXCR4.

The potential of the CXCR4 Nanobodies to antagonize CXCL12-dependent signaling was evaluated in multiple functional assays that reflect divergent CXCR4 signaling routes or differences in the extent of signal amplification (2^{nd} messenger levels vs gene regulation). In general, each antagonist was equipotent and equieffective in antagonizing either CXCR4-WT or the CXCR4-WHIM receptors. The Nanobodies showed higher potencies in inhibiting CXCL12-induced $G\alpha_i$ activation, as compared to AMD3100, with IC_{50} values that reflect their binding affinities. Also, in the cAMP reporter assay, the bivalent nanobody was significantly more potent than AMD3100. After these initial signaling studies in HEK293T cells, the Nanobodies were further validated in clinically more relevant, WHIM-related cell lines. In leukemic K562 cells, the CXCL12-induced calcium flux, mediated by either CXCR4-WT or CXCR4-R334X, was inhibited by both the Nanobodies and AMD3100. WHIM syndrome is often clinically characterized by HPV-associated warts and carcinogenesis. Such manifestations might be directly related to aberrant CXCR4-WHIM signaling, as suggested by the interplay between the CXCL12 signaling axis and the HPV life cycle (Chow et al., 2010; Meuris et al., 2016). Such interplay is notably manifested by the

JPET Fast Forward. Published on August 2, 2017 as DOI: 10.1124/jpet.117.242735
This article has not been copyedited and formatted. The final version may differ from this version.

CXCL12-dependency of HPV-immortalized keratinocytes migration, which can be measured in a wound healing assay (Chow et al., 2010). We found that the nanobody dose-dependently inhibited the wound healing in HPV-immortalized keratinocytes up to 61%, whereas AMD3100 inhibited only 26% of the wound. Taken together, our functional experiments demonstrate that these new CXCR4 Nanobodies effectively inhibit CXCL12-dependent CXCR4 signaling with potencies that are superior of that of AMD3100.

Because of the small size and modular structure of Nanobodies, multivalent nanobody constructs are easily generated. Therefore, in order to extend the half-life of the Nanobodies in the blood circulation, target-specific Nanobodies are often coupled to Nanobodies directed against human- or murine albumin (Roovers et al., 2007; Tijink et al., 2008). This half-life extension (HLE) can increase the half-life of the Nanobodies in blood up several days (Tijink et al., 2008). For example, in clinical tests, IL6-receptor Nanobodies that have been modified accordingly, showed serum half-life of several weeks and therapeutic outcome upon weekly administration (Van Roy et al., 2015). In contrast, AMD3100 is associated with poor pharmacokinetics (blood half-life of only a few hours) forcing its administration to WHIM patients twice a day (Hendrix et al., 2000; McDermott et al., 2014b). Half-life extended variants of CXCR7-specific Nanobodies were described previously (Maussang et al., 2013). Similar modification of the CXCR4 Nanobodies from this study would render them as potent alternatives for treatment of CXCR4-related diseases.

In recent years the nanobody platform has been gaining ground in GPCR-research as therapeutics, diagnostics and research tools (Mujic-Delic et al., 2014; Manglik et al., 2017). Being stable proteins, Nanobodies can be readily tagged with fluorescent-probes, radiolabels or epitope-tags and thus utilized for CXCR4 detection, imaging and diagnostic purposes (e.g. ELISA, immunohistochemistry, immunofluorescence) or as crystallization chaperones (Mujic-Delic et al., 2014; Manglik et al., 2017). Being specific for human CXCR4 allows for detection of human CXCR4-expressing cells in human xenografts in animal experiments or detection of CXCR4 in immunohistochemistry on patient samples. However, future testing of Nanobodies in an *in vivo* WHIM model, such as the *Cxcr4*$^{+/mutant(1013)}$ model (the

WHIM syndrome-associated CXCR4-S338X mutation) (Balabanian et al., 2012), would require mouse reactive Nanobodies. Furthermore, the extracellular localization of the binding epitope of these Nanobodies allows them to be used as targeting ligands in non-invasive imaging techniques, such as near-infra-red (NIR) or positron emission tomography (PET) imaging or for the delivery of therapeutic pay-loads to CXCR4-expressing cells (Oliveira et al., 2013).

In conclusion, these data illustrate that the bivalent CXCR4-targeting nanobody 10A10-10A10 is highly potent in inhibiting CXCL12/CXCR4 signaling. Importantly, their modularity and HLE make these Nanobodies a promising alternative to AMD3100 for CXCR4-related diseases like WHIM syndrome and Waldenström's macroglobulinemia.

ACKNOWLEDGEMENTS

The authors thank David McDermott and Philip Murphy for the discussions and providing the K562 cell lines. H.F.V., F.B and M.J.S. are part of the European Union's Horizon2020 MSCA Programme under grant agreement 641833 (ONCORNET).

AUTHORSHIP CONTRIBUTIONS

Participated in research design: de Wit, Maussang, Cutolo, Bachelerie, Smit

Conducted experiments: de Wit, Brink, Arsova, Cutolo

Contributed new reagents or analytic tools: Strubbe

Performed data analysis: de Wit, Heukers, Brink, Cutolo

Wrote or contributed to the writing of the manuscript: de Wit, Heukers, Bachelerie, Vischer, Smit

REFERENCES

Al Ustwani O, Kurzrock R and Wetzler M (2014) Genetics on a WHIM. *Br J Haematol* **164**:15-23.

Bachelerie F (2010) CXCL12/CXCR4-axis dysfunctions: Markers of the rare immunodeficiency disorder WHIM syndrome. *Dis Markers* **29**:189-198.

Balabanian K, Brotin E, Biajoux V, Bouchet-Delbos L, Lainey E, Fenneteau O, Bonnet D, Fiette L, Emilie D and Bachelerie F (2012) Proper desensitization of CXCR4 is required for lymphocyte development and peripheral compartmentalization in mice. *Blood* **119**:5722-5730.

Balabanian K, Lagane B, Pablos JL, Laurent L, Planchenault T, Verola O, Lebbe C, Kerob D, Dupuy A, Hermine O, Nicolas JF, Latger-Cannard V, Bensoussan D, Bordigoni P, Baleux F, Le Deist F, Virelizier JL, Arenzana-Seisdedos F and Bachelerie F (2005) WHIM syndromes with different genetic anomalies are accounted for by impaired CXCR4 desensitization to CXCL12. *Blood* **105**:2449-2457.

Ballester LY, Loghavi S, Kanagal-Shamanna R, Barkoh BA, Lin P, Medeiros LJ, Luthra R and Patel KP (2016) Clinical Validation of a CXCR4 Mutation Screening Assay for Waldenstrom Macroglobulinemia. *Clinical lymphoma, myeloma & leukemia* **16**:395-403.e391.

Beaussant Cohen S, Fenneteau O, Plouvier E, Rohrlich PS, Daltroff G, Plantier I, Dupuy A, Kerob D, Beaupain B, Bordigoni P, Fouyssac F, Delezoide AL, Devouassoux G, Nicolas JF, Bensaid P, Bertrand Y, Balabanian K, Chantelot CB, Bachelerie F and Donadieu J (2012) Description and outcome of a cohort of 8 patients with WHIM syndrome from the French Severe Chronic Neutropenia Registry. *Orphanet J Rare Dis* **7**:71.

Biajoux V, Natt J, Freitas C, Alouche N, Sacquin A, Hemon P, Gaudin F, Fazilleau N, Espeli M and Balabanian K (2016) Efficient Plasma Cell Differentiation and Trafficking Require Cxcr4 Desensitization. *Cell Rep* **17**:193-205.

Bock I, Dugue F, Loppinet E, Bellanne-Chantelot C and Benet B (2014) [WHIM syndrome: presumptive diagnosis based on myelokathexis on bone marrow smear]. *Annales de biologie clinique* **72**:111-119.

Brault L, Rovo A, Decker S, Dierks C, Tzankov A and Schwaller J (2014) CXCR4-SERINE339 regulates cellular adhesion, retention and mobilization, and is a marker for poor prognosis in acute myeloid leukemia. *Leukemia* **28**:566-576.

Brelot A, Heveker N, Montes M and Alizon M (2000) Identification of residues of CXCR4 critical for human immunodeficiency virus coreceptor and chemokine receptor activities. *The Journal of biological chemistry* **275**:23736-23744.

Cao Y, Hunter ZR, Liu X, Xu L, Yang G, Chen J, Patterson CJ, Tsakmaklis N, Kanan S, Rodig S, Castillo JJ and Treon SP (2015) The WHIM-like CXCR4(S338X) somatic mutation activates AKT and ERK, and promotes resistance to ibrutinib and other agents used in the treatment of Waldenstrom's Macroglobulinemia. *Leukemia* **29**:169-176.

Chow KY, Brotin E, Ben Khalifa Y, Carthagena L, Teissier S, Danckaert A, Galzi JL, Arenzana-Seisdedos F, Thierry F and Bachelerie F (2010) A pivotal role for CXCL12 signaling in HPV-mediated transformation of keratinocytes: clues to understanding HPV-pathogenesis in WHIM syndrome. *Cell Host Microbe* **8**:523-533.

Conklin BR, Farfel Z, Lustig KD, Julius D and Bourne HR (1993) Substitution of three amino acids switches receptor specificity of Gq alpha to that of Gi alpha. *Nature* **363**:274-276.

Cutolo P, Basdevant N, Bernadat G, Bachelerie F and Ha-Duong T (2017) Interaction of chemokine receptor CXCR4 in monomeric and dimeric state with its endogenous ligand CXCL12: coarse-grained simulations identify differences. *Journal of biomolecular structure & dynamics* **35**:399-412.

Dale DC, Bolyard AA, Kelley ML, Westrup EC, Makaryan V, Aprikyan A, Wood B and Hsu FJ (2011) The CXCR4 antagonist plerixafor is a potential therapy for myelokathexis, WHIM syndrome. *Blood* **118**:4963-4966.

De Clercq E (2003) The bicyclam AMD3100 story. *Nature reviews Drug discovery* **2**:581-587.

de Wit RH, de Munnik SM, Leurs R, Vischer HF and Smit MJ (2016) Molecular Pharmacology of Chemokine Receptors. *Methods in enzymology* **570**:457-515.

Devine SM, Flomenberg N, Vesole DH, Liesveld J, Weisdorf D, Badel K, Calandra G and DiPersio JF (2004) Rapid mobilization of CD34+ cells following administration of the CXCR4 antagonist AMD3100 to patients with multiple myeloma and non-Hodgkin's lymphoma. *J Clin Oncol* **22**:1095-1102.

Els Conrath K, Lauwereys M, Wyns L and Muyldermans S (2001) Camel single-domain antibodies as modular building units in bispecific and bivalent antibody constructs. *The Journal of biological chemistry* **276**:7346-7350.

Forster R, Kremmer E, Schubel A, Breitfeld D, Kleinschmidt A, Nerl C, Bernhardt G and Lipp M (1998) Intracellular and surface expression of the HIV-1 coreceptor CXCR4/fusin on various leukocyte subsets: rapid internalization and recycling upon activation. *Journal of immunology* **160**:1522-1531.

Freitas C, Wittner M, Nguyen J, Rondeau V, Biajoux V, Aknin ML, Gaudin F, Beaussant-Cohen S, Bertrand Y, Bellanne-Chantelot C, Donadieu J, Bachelerie F, Espeli M, Dalloul A, Louache F and Balabanian K (2017) Lymphoid differentiation of hematopoietic stem cells requires efficient Cxcr4 desensitization. *J Exp Med*.

Gorlin RJ, Gelb B, Diaz GA, Lofsness KG, Pittelkow MR and Fenyk JR, Jr. (2000) WHIM syndrome, an autosomal dominant disorder: clinical, hematological, and molecular studies. *American journal of medical genetics* **91**:368-376.

Gravel S, Malouf C, Boulais PE, Berchiche YA, Oishi S, Fujii N, Leduc R, Sinnett D and Heveker N (2010) The peptidomimetic CXCR4 antagonist TC14012 recruits beta-arrestin to CXCR7: roles of receptor domains. *The Journal of biological chemistry* **285**:37939-37943.

Hendrix CW, Flexner C, MacFarland RT, Giandomenico C, Fuchs EJ, Redpath E, Bridger G and Henson GW (2000) Pharmacokinetics and safety of AMD-3100, a novel antagonist of the CXCR-4 chemokine receptor, in human volunteers. *Antimicrob Agents Chemother* **44**:1667-1673.

Hernandez PA, Gorlin RJ, Lukens JN, Taniuchi S, Bohinjec J, Francois F, Klotman ME and Diaz GA (2003) Mutations in the chemokine receptor gene CXCR4 are associated with WHIM syndrome, a combined immunodeficiency disease. *Nature genetics* **34**:70-74.

Hunter ZR, Xu L, Yang G, Zhou Y, Liu X, Cao Y, Manning RJ, Tripsas C, Patterson CJ, Sheehy P and Treon SP (2014) The genomic landscape of Waldenstrom macroglobulinemia is characterized by highly recurring MYD88 and WHIM-like CXCR4 mutations, and small somatic deletions associated with B-cell lymphomagenesis. *Blood* **123**:1637-1646.

Imashuku S, Miyagawa A, Chiyonobu T, Ishida H, Yoshihara T, Teramura T, Kuriyama K, Imamura T, Hibi S, Morimoto A and Todo S (2002) Epstein-Barr virus-associated T-lymphoproliferative disease with hemophagocytic syndrome, followed by fatal intestinal B lymphoma in a young adult female with WHIM syndrome. Warts, hypogammaglobulinemia, infections, and myelokathexis. *Ann Hematol* **81**:470-473.

Jahnichen S, Blanchetot C, Maussang D, Gonzalez-Pajuelo M, Chow KY, Bosch L, De Vrieze S, Serruys B, Ulrichts H, Vandevelde W, Saunders M, De Haard HJ, Schols D, Leurs R, Vanlandschoot P, Verrips T and Smit MJ (2010) CXCR4 nanobodies (VHH-based single variable domains) potently inhibit chemotaxis and HIV-1 replication and mobilize stem cells. *Proceedings of the National Academy of Sciences of the United States of America* **107**:20565-20570.

Kallikourdis M, Trovato AE, Anselmi F, Sarukhan A, Roselli G, Tassone L, Badolato R and Viola A (2013) The CXCR4 mutations in WHIM syndrome impair the stability of the T-cell immunologic synapse. *Blood* **122**:666-673.

Kapoor P, Paludo J, Vallumsetla N and Greipp PR (2015) Waldenstrom macroglobulinemia: What a hematologist needs to know. *Blood Rev* **29**:301-319.

Kawai T and Malech HL (2009) WHIM syndrome: congenital immune deficiency disease. *Current opinion in hematology* **16**:20-26.

Lagane B, Chow KY, Balabanian K, Levoye A, Harriague J, Planchenault T, Baleux F, Gunera-Saad N, Arenzana-Seisdedos F and Bachelerie F (2008) CXCR4 dimerization and beta-arrestin-mediated signaling account for the enhanced chemotaxis to CXCL12 in WHIM syndrome. *Blood* **112**:34-44.

Lee B, Sharron M, Montaner LJ, Weissman D and Doms RW (1999) Quantification of CD4, CCR5, and CXCR4 levels on lymphocyte subsets, dendritic cells, and differentially conditioned monocyte-derived macrophages. *Proceedings of the National Academy of Sciences of the United States of America* **96**:5215-5220.

Liles WC, Broxmeyer HE, Rodger E, Wood B, Hubel K, Cooper S, Hangoc G, Bridger GJ, Henson GW, Calandra G and Dale DC (2003) Mobilization of hematopoietic progenitor cells in healthy volunteers by AMD3100, a CXCR4 antagonist. *Blood* **102**:2728-2730.

Liu Q, Chen H, Ojode T, Gao X, Anaya-O'Brien S, Turner NA, Ulrick J, DeCastro R, Kelly C, Cardones AR, Gold SH, Hwang EI, Wechsler DS, Malech HL, Murphy PM and McDermott DH (2012) WHIM syndrome caused by a single amino acid substitution in the carboxy-tail of chemokine receptor CXCR4. *Blood* **120**:181-189.

Liu Q, Pan C, Lopez L, Gao J, Velez D, Anaya-O'Brien S, Ulrick J, Littel P, Corns JS, Ellenburg DT, Malech HL, Murphy PM and McDermott DH (2016) WHIM Syndrome Caused by Waldenstrom's Macroglobulinemia-Associated Mutation CXCR4 (L329fs). *J Clin Immunol* **36**:397-405.

Ma Q, Jones D and Springer TA (1999) The chemokine receptor CXCR4 is required for the retention of B lineage and granulocytic precursors within the bone marrow microenvironment. *Immunity* **10**:463-471.

Manglik A, Kobilka BK and Steyaert J (2017) Nanobodies to Study G Protein-Coupled Receptor Structure and Function. *Annual review of pharmacology and toxicology* **57**:19-37.

Maussang D, Mujic-Delic A, Descamps FJ, Stortelers C, Vanlandschoot P, Stigter-van Walsum M, Vischer HF, van Roy M, Vosjan M, Gonzalez-Pajuelo M, van Dongen GA, Merchiers P, van Rompaey P and Smit MJ (2013) Llama-derived single variable domains (nanobodies) directed against chemokine receptor CXCR7 reduce head and neck cancer cell growth in vivo. *The Journal of biological chemistry* **288**:29562-29572.

McCormick PJ, Segarra M, Gasperini P, Gulino AV and Tosato G (2009) Impaired recruitment of Grk6 and beta-Arrestin 2 causes delayed internalization and desensitization of a WHIM syndrome-associated CXCR4 mutant receptor. *PloS one* **4**:e8102.

McDermott DH, Gao JL, Liu Q, Siwicki M, Martens C, Jacobs P, Velez D, Yim E, Bryke CR, Hsu N, Dai Z, Marquesen MM, Stregevsky E, Kwatemaa N, Theobald N, Long Priel DA, Pittaluga S, Raffeld MA, Calvo KR, Maric I, Desmond R, Holmes KL, Kuhns DB, Balabanian K, Bachelerie F, Porcella SF, Malech HL and Murphy PM (2015) Chromothriptic cure of WHIM syndrome. *Cell* **160**:686-699.

McDermott DH, Liu Q, Ulrick J, Kwatemaa N, Anaya-O'Brien S, Penzak SR, Filho JO, Priel DA, Kelly C, Garofalo M, Littel P, Marquesen MM, Hilligoss D, Decastro R, Fleisher TA, Kuhns DB, Malech HL and Murphy PM (2011a) The CXCR4 antagonist plerixafor corrects panleukopenia in patients with WHIM syndrome. *Blood* **118**:4957-4962.

McDermott DH, Liu Q, Velez D, Lopez L, Anaya-O'Brien S, Ulrick J, Kwatemaa N, Starling J, Fleisher TA, Priel DA, Merideth MA, Giuntoli RL, Evbuomwan MO, Littel P, Marquesen MM, Hilligoss D, DeCastro R, Grimes GJ, Hwang ST, Pittaluga S, Calvo KR, Stratton P, Cowen EW, Kuhns DB, Malech HL and Murphy PM (2014a) A phase 1 clinical trial of long-term, low-dose treatment of WHIM syndrome with the CXCR4 antagonist plerixafor. *Blood* **123**:2308-2316.

McDermott DH, Liu Q, Velez D, Lopez L, Anaya-O'Brien S, Ulrick J, Kwatemaa N, Starling J, Fleisher TA, Priel DAL, Merideth MA, Giuntoli RL, Evbuomwan MO, Littel P, Marquesen MM, Hilligoss D, DeCastro R, Grimes GJ, Hwang ST, Pittaluga S, Calvo KR, Stratton P, Cowen EW, Kuhns DB, Malech HL and

Murphy PM (2014b) A phase 1 clinical trial of long-term, low-dose treatment of WHIM syndrome with the CXCR4 antagonist plerixafor. *Blood* **123**:2308-2316.

McDermott DH, Lopez J, Deng F, Liu Q, Ojode T, Chen H, Ulrick J, Kwatemaa N, Kelly C, Anaya-O'Brien S, Garofalo M, Marquesen M, Hilligoss D, DeCastro R, Malech HL and Murphy PM (2011b) AMD3100 is a potent antagonist at CXCR4(R334X) , a hyperfunctional mutant chemokine receptor and cause of WHIM syndrome. *J Cell Mol Med* **15**:2071-2081.

Meuris F, Carthagena L, Jaracz-Ros A, Gaudin F, Cutolo P, Deback C, Xue Y, Thierry F, Doorbar J and Bachelerie F (2016) The CXCL12/CXCR4 Signaling Pathway: A New Susceptibility Factor in Human Papillomavirus Pathogenesis. *PLoS Pathog* **12**:e1006039.

Mueller W, Schutz D, Nagel F, Schulz S and Stumm R (2013) Hierarchical organization of multi-site phosphorylation at the CXCR4 C terminus. *PloS one* **8**:e64975.

Mujic-Delic A, de Wit RH, Verkaar F and Smit MJ (2014) GPCR-targeting nanobodies: attractive research tools, diagnostics, and therapeutics. *Trends in pharmacological sciences* **35**:247-255.

Oliveira S, Heukers R, Sornkom J, Kok RJ and van Bergen En Henegouwen PM (2013) Targeting tumors with nanobodies for cancer imaging and therapy. *J Control Release* **172**:607-617.

Peyvandi F, Scully M, Kremer Hovinga JA, Cataland S, Knobl P, Wu H, Artoni A, Westwood JP, Mansouri Taleghani M, Jilma B, Callewaert F, Ulrichts H, Duby C and Tersago D (2016) Caplacizumab for Acquired Thrombotic Thrombocytopenic Purpura. *N Engl J Med* **374**:511-522.

Roccaro AM, Sacco A, Jimenez C, Maiso P, Moschetta M, Mishima Y, Aljawai Y, Sahin I, Kuhne M, Cardarelli P, Cohen L, San Miguel JF, Garcia-Sanz R and Ghobrial IM (2014) C1013G/CXCR4 acts as a driver mutation of tumor progression and modulator of drug resistance in lymphoplasmacytic lymphoma. *Blood* **123**:4120-4131.

Roovers RC, Laeremans T, Huang L, De Taeye S, Verkleij AJ, Revets H, de Haard HJ and van Bergen en Henegouwen PM (2007) Efficient inhibition of EGFR signaling and of tumour growth by antagonistic anti-EFGR Nanobodies. *Cancer immunology, immunotherapy : CII* **56**:303-317.

Rudnick SI and Adams GP (2009) Affinity and avidity in antibody-based tumor targeting. *Cancer biotherapy & radiopharmaceuticals* **24**:155-161.

Schlaeger EJ and Christensen K (1999) Transient gene expression in mammalian cells grown in serum-free suspension culture. *Cytotechnology* **30**:71-83.

Scozzafava A, Mastrolorenzo A and Supuran CT (2002) Non-peptidic chemokine receptors antagonists as emerging anti-HIV agents. *J Enzyme Inhib Med Chem* **17**:69-76.

Steyaert J and Kobilka BK (2011) Nanobody stabilization of G protein-coupled receptor conformational states. *Current opinion in structural biology* **21**:567-572.

Tijink BM, Laeremans T, Budde M, Stigter-van Walsum M, Dreier T, de Haard HJ, Leemans CR and van Dongen GA (2008) Improved tumor targeting of anti-epidermal growth factor receptor Nanobodies through albumin binding: taking advantage of modular Nanobody technology. *Mol Cancer Ther* **7**:2288-2297.

Van Roy M, Ververken C, Beirnaert E, Hoefman S, Kolkman J, Vierboom M, Breedveld E, t Hart B, Poelmans S, Bontinck L, Hemeryck A, Jacobs S, Baumeister J and Ulrichts H (2015) The preclinical pharmacology of the high affinity anti-IL-6R Nanobody(R) ALX-0061 supports its clinical development in rheumatoid arthritis. *Arthritis research & therapy* **17**:135.

Vauquelin G and Charlton SJ (2013) Exploring avidity: understanding the potential gains in functional affinity and target residence time of bivalent and heterobivalent ligands. *British journal of pharmacology* **168**:1771-1785.

Wang ZX, Berson JF, Zhang TY, Cen YH, Sun Y, Sharron M, Lu ZH and Peiper SC (1998) CXCR4 sequences involved in coreceptor determination of human immunodeficiency virus type-1 tropism. Unmasking of activity with M-tropic Env glycoproteins. *The Journal of biological chemistry* **273**:15007-15015.

Wescott MP, Kufareva I, Paes C, Goodman JR, Thaker Y, Puffer BA, Berdougo E, Rucker JB, Handel TM and Doranz BJ (2016) Signal transmission through the CXC chemokine receptor 4 (CXCR4) transmembrane helices. *Proceedings of the National Academy of Sciences of the United States of America* **113**:9928-9933.

Yoshii Y, Kato T, Ono K, Takahashi E, Fujimoto N, Kobayashi S, Kimura F, Nonoyama S and Satoh T (2015) Primary cutaneous follicle center lymphoma in a patient with WHIM syndrome. *Journal of the European Academy of Dermatology and Venereology : JEADV*.

Footnotes:

This work was supported by the Netherlands Organization for Scientific Research (NWO: Vici grant) and the Dutch Technology Foundation (STW).

[1]Current affiliation: Department of Drug Design and Pharmacology, Faculty of Health and Medical Sciences, University of Copenhagen, Copenhagen, Denmark

[2]Current affiliation: Merus N.V., Utrecht, The Netherlands

JPET Fast Forward. Published on August 2, 2017 as DOI: 10.1124/jpet.117.242735
This article has not been copyedited and formatted. The final version may differ from this version.

Figure legends

Figure 1. WHIM mutation in CXCR4 sustains CXCL12-induced signaling. A) Binding of ^{125}I-labeled CXCL12 to HEK293T membranes containing either WT CXCR4 (closed circles) or two WHIM mutants R334X (open squares) and S338X (open triangles). B) CXCL12-induced accumulation of [^{3}H]-inositol phosphates in HEK293T cells expressing either CXCR4-WT or the WHIM mutants R334X or S338X. CXCR4-mediated PLC activation was obtained by co-expression with $G\alpha_{qi5}$. Plotted are means with SEM. C) Expression levels of CXCR4-WT or CXCR4-S338X, as determined using 12G5 antibody in a cell surface expression ELISA. D) CXCL12-induced phosphorylation of ERK1/2 at threonine 202 and tyrosine 204, as determined by western blotting. HEK293T cells expressing either CXCR4-WT or the WHIM mutant S338X were treated with CXCL12 (100 nM) for 5 or 15 minutes. Total ERK1/2 was stained as loading control.

Figure 2. Nanobodies displace CXCL12 from CXCR4-WT and WHIM mutants via binding to ECL2 of the receptor. A) Binding of 10A10-10A10 (100 nM) to HEK293T cells expressing CXCR4-WT or WHIM mutant R334X, as determined by immunofluorescence microscopy. B) Binding of ^{125}I-labeled CXCL12 (75 pM) to HEK293T membranes containing either CXCR4-WT (left) or WHIM mutant R334X (right) in the presence of a concentration range of AMD3100 (closed circles), 10A10 (open circles), 10A10-10A10 (open squares). C) Binding of ^{125}I-CXCL12 to HEK293T membranes expressing either human- or mouse CXCR4 or human ACKR3/CXCR7 in the presence of an excess of unlabeled CXCL12 (100 nM, black) or 10A10 (1 µM, grey). D) Snake plot depicting the extracellular loop 2 (ECL2) of human CXCR4 (top) or mouse CXCR4 (bottom). The three residues that were mutated for epitope mapping (D187, F189 and V196) are indicated in black. E) Binding of a concentration range of 10A10-10A10 to HEK293T cells expressing either CXCR4-WT (filled circles) or the CXCR4 ECL2 mutants D187V (open squares, F189V (open triangles) or V196E (open inverted triangles), as determined by flow cytometry. Plotted are means with SEM.

JPET Fast Forward. Published on August 2, 2017 as DOI: 10.1124/jpet.117.242735
This article has not been copyedited and formatted. The final version may differ from this version.

Figure 3. Nanobodies inhibit CXCL12-induced signaling mediated by CXCR4-WT and WHIM mutants. A) Inhibition of CXCL12-induced (5 nM) accumulation of [^{3}H]-inositol phosphates in HEK293T cells expressing CXCR4-WT or the WHIM mutant R334X (dashed line) by a concentration range of AMD3100 (filled circles) or 10A10-10A10 (open squares). CXCR4-mediated PLC activation was obtained by co-expression with $G\alpha_{qi5}$. B) Inhibition of CXCL12-induced (1 nM) phosphorylation of ERK1/2 by AMD3100 (1 µM) and 10A10-10A10 (100 nM) in HEK293T expressing CXCR4-WT (top) or the WHIM mutant R334X (bottom), as determined by western blot. Total ERK1/2 was stained as loading control. C-D) Inhibition of CXCL12-induced CRE activation by concentration ranges of AMD3100 (filled circles) or 10A10-10A10 (open squares) in HEK293T cells expressing CXCR4-WT (C) or the WHIM mutant R334X. Values were plotted in percentages of maximal effect where 0% represents the response to 1 nM of CXCL12 and 100% represents 1 µM of forskolin (D). Plotted are means with SEM.

Figure 4. Nanobody-mediated inhibition of CXCR4 signaling in WHIM-related disease model systems. A) Real-time calcium flux responses in myleoid leukemic K562 cells (open circles) expressing CXCR4-WT (closed circles) or WHIM mutant R334X (open squares). Cells were treated with CXCL12 (5 nM, black arrow) and intracellular calcium release was monitored by measuring the fluorescence intensity of Fluor-4 NW dye. B) Inhibition of CXCL12-induced (5 nM) calcium flux in K562 cells expressing CXCR WT (left) or WHIM mutant R334X (right) by nanobody 10A10-10A10 (100 nM) or AMD3100 (10 µM). C-D) Inhibition of wound healing by a concentration range of 10A10-10A10 or AMD3100 (25 µM) using HPV18-immortalized human keratinocytes. Wound healing was monitored for 16 h in the presence of the inhibitors and the degree of wound healing was calculated as percentage of total gap closure. Plotted are means with SEM.

JPET Fast Forward. Published on August 2, 2017 as DOI: 10.1124/jpet.117.242735
This article has not been copyedited and formatted. The final version may differ from this version.

Table I: Alignment of CXCR4-WT and WHIM C-terminal amino acid (aa) sequences

CXCR4	C-terminal sequence
WT	SV SRGSSLKILS KGKRGGHSSV STESESSSFH SS
R334X	SV SRGSSLKILS KGK
S338X	SV SRGSSLKILS KGKRGGH
	| | | |
aa	320 330 340 350

JPET Fast Forward. Published on August 2, 2017 as DOI: 10.1124/jpet.117.242735
This article has not been copyedited and formatted. The final version may differ from this version.

Table II: Pharmacological characteristics of CXCR4-antagonists

		CXCR4	10A10	10A10-10A10	AMD3100
Ligand displacement (^{125}I-CXCL12)	Binding inhibition potency (pIC_{50} ± SEM)	WT	7.58 ± 0.08	9.08 ± 0.15	6.36 ± 0.09
		R334X	7.83 ± 0.07	8.97 ± 0.03	6.35 ± 0.13
		S338X	7.68 ± 0.11	9.13 ± 0.17	6.53 ± 0.05
Binding (Flow cytometry)	Affinity (pK_d ± SEM)	WT	n.d.	8.87 ± 0.06	n.d.
		D187V		-	
		F189V		8.75 ± 0.03	
		V196E		8.00 ± 0.03	
$G\alpha_i$ activation (InsP accumulation)	Potency (pIC_{50} ± SEM)	WT	7.92 ± 0.03	8.28 ± 0.04	6.17 ± 0.03
		R334X	7.94 ± 0.03	8.30 ± 0.06	6.24 ± 0.16
		S338X	7.94 ± 0.06	8.28 ± 0.05	6.22 ± 0.07
cAMP (CRE reporter)	Potency (pIC_{50} ± SEM)	WT	6.8 ± 0.1	8.0 ± 0.1	6.7 ± 0.2
		R334X	7.0 ± 0.1	7.9 ± 0.1	7.3 ± 0.1
		S338X	7.0 ± 0.1	7.6 ± 0.1	7.2 ± 0.1
	CXCL12 inhibition (% ± SEM)	WT	77 ± 13	107 ±9	71 ± 15
		R334X	84 ± 10	109 ± 10	64 ± 9
		S338X	78 ± 10	103 ± 14	61 ± 10
Ca flux	CXCL12 inhibition (% ± SEM)	WT	n.d.	93 ± 2	96 ± 1
		R334X		70 ± 9	83 ± 4

JPET Fast Forward. Published on August 2, 2017 as DOI: 10.1124/jpet.117.242735
This article has not been copyedited and formatted. The final version may differ from this version.

Supplemental Figure 1. Inhibition of CXCL12 binding in CXCL12-induced signaling in CXCR4 WHIM mutant S338X. A) Basal and CXCL12-induced (5 nM) [^{3}H]-inositol phosphates accumulation of Mock ($G\alpha_{qi5}$-only transfection), CXCR4-WT, CXCR4-R334X or CXCR-R338X expressing HEK293T cells. B) Binding of ^{125}I-labeled CXCL12 (75 pM) to HEK293T membranes containing CXCR4 WHIM mutant S338X in the presence of a concentration range of AMD3100 (closed circles), 10A10 (open circles), 10A10-10A10 (open squares). C) CXCL12-induced (5 nM) accumulation of [^{3}H]-inositol phosphates in HEK293T cells expressing CXCR4 WHIM mutant S338X by a concentration range of AMD3100 (filled circles) or 10A10-10A10 (open squares). CXCR4-mediated PLC activation was obtained by co-expression with $G\alpha_{qi5}$. D) CXCL12-induced CRE activation in HEK293T cells expressing CXCR4 wild type or the WHIM mutants R334X or S338X, as determined by CRE-luciferase reporter gene assay. E) Inhibition of CXCL12-induced CRE activation by a concentration range of AMD3100 (filled circles) or 10A10-10A10 (open squares). Plotted are mean with SEM of a representative graph, n = 3.

JPET Fast Forward. Published on August 2, 2017 as DOI: 10.1124/jpet.117.242735
This article has not been copyedited and formatted. The final version may differ from this version.

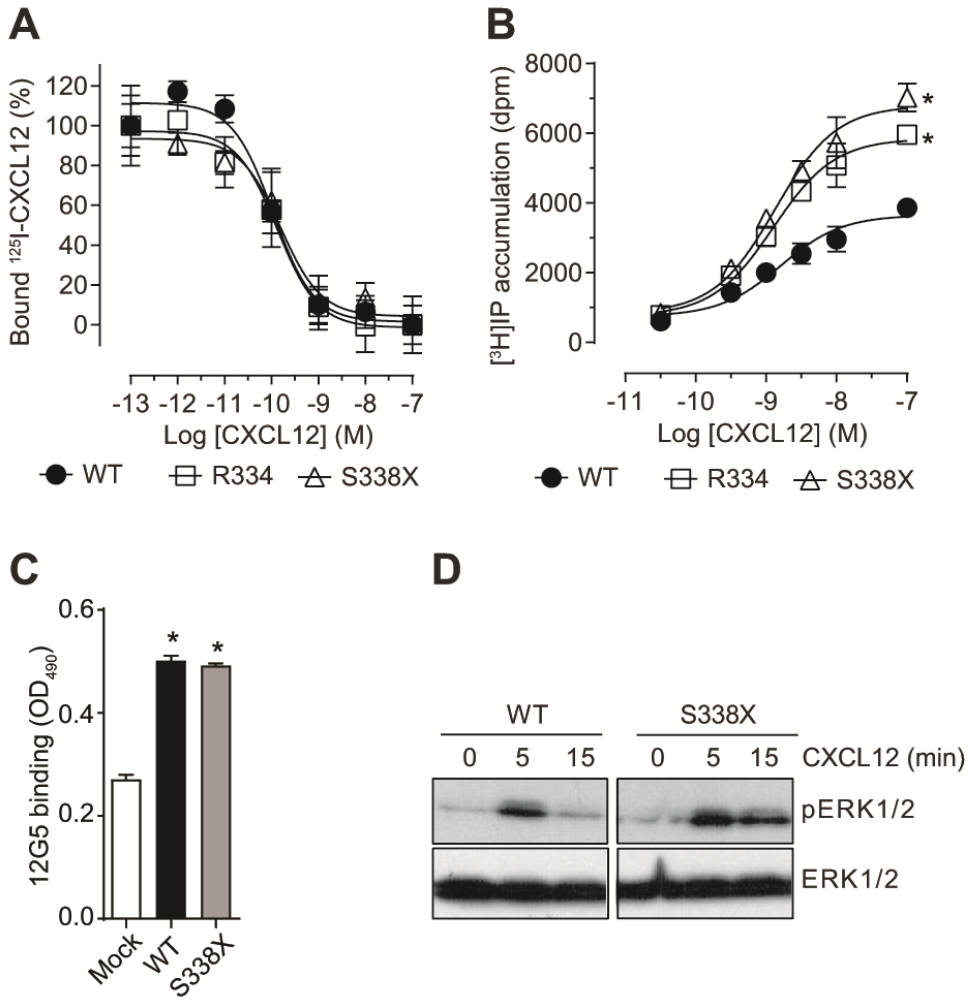

Figure 1

JPET Fast Forward. Published on August 2, 2017 as DOI: 10.1124/jpet.117.242735
This article has not been copyedited and formatted. The final version may differ from this version.

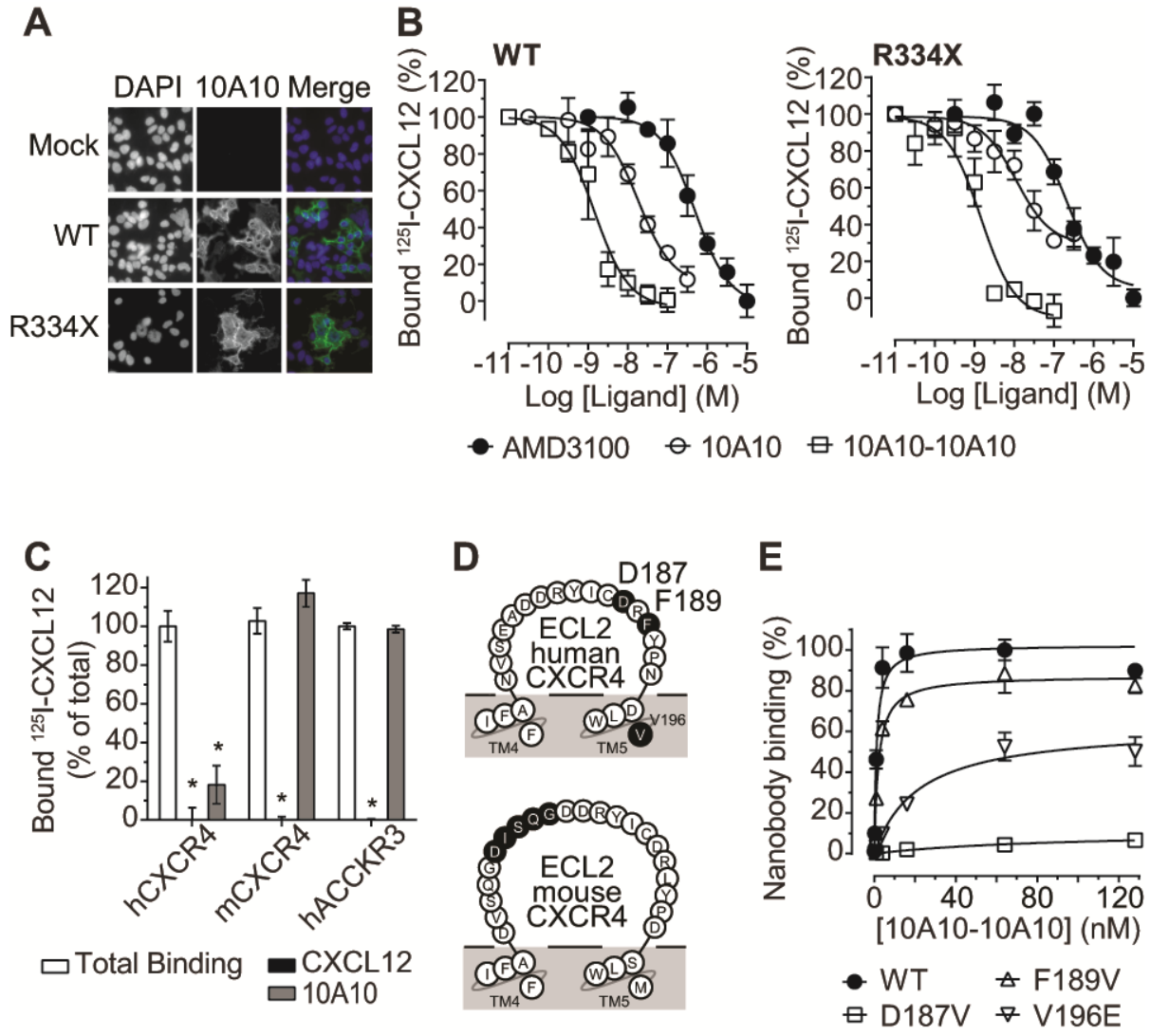

Figure 2

JPET Fast Forward. Published on August 2, 2017 as DOI: 10.1124/jpet.117.242735
This article has not been copyedited and formatted. The final version may differ from this version.

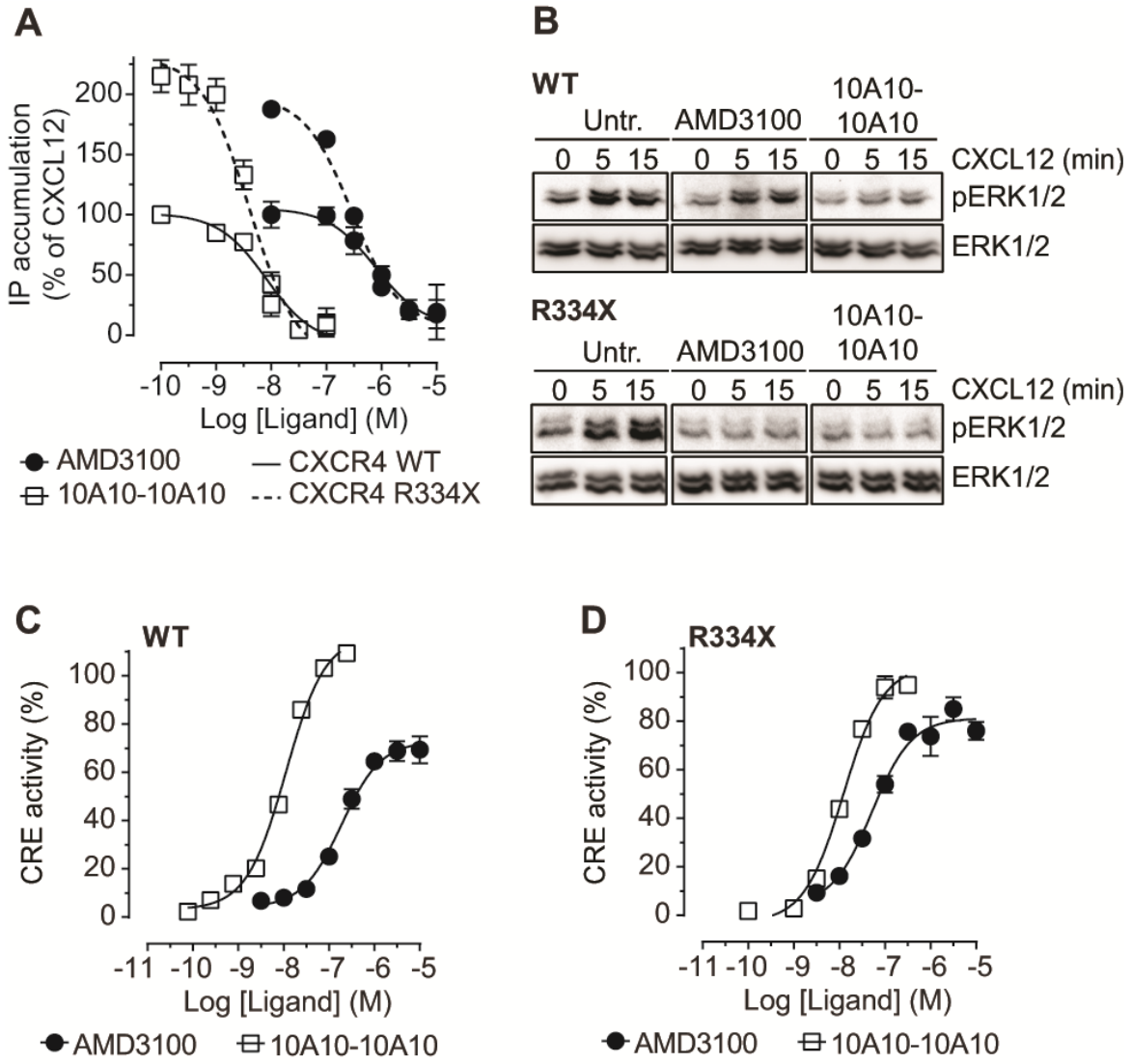

Figure 3

JPET Fast Forward. Published on August 2, 2017 as DOI: 10.1124/jpet.117.242735
This article has not been copyedited and formatted. The final version may differ from this version.

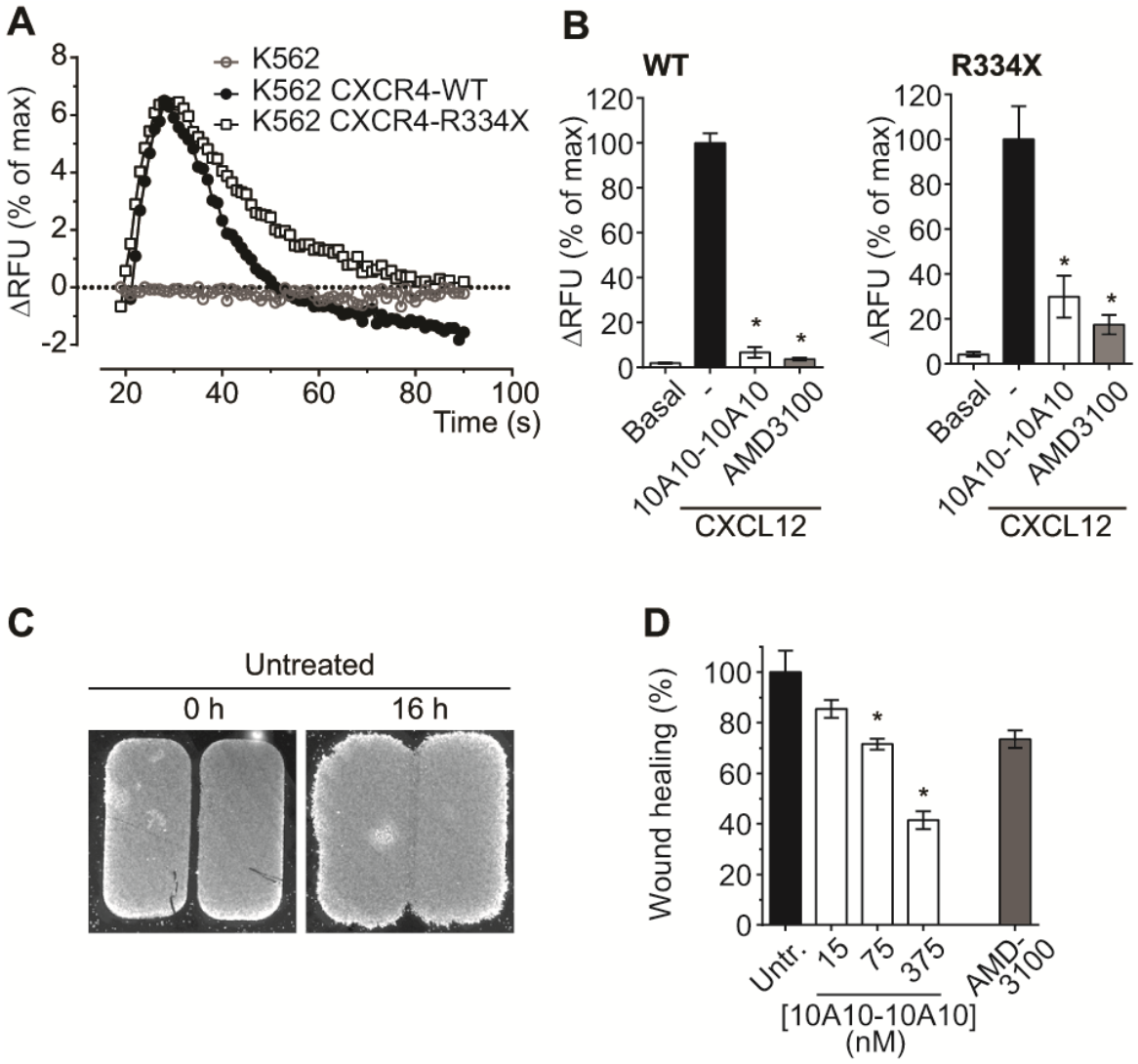

Figure 4